RESEARCH ARTICLE

WILEY

Dynamic transient brain states in preschoolers mirror parental report of behavior and emotion regulation

Lisa Toffoli[1] | Natalia Zdorovtsova[2] | Gabriela Epihova[2] |
Gian Marco Duma[3] | Fiorella Del Popolo Cristaldi[1] | Massimiliano Pastore[4] |
Duncan E. Astle[2,5] | Giovanni Mento[1,3]

[1]NeuroDev Lab, Department of General Psychology, University of Padua, Padua, Italy

[2]MRC Cognition and Brain Sciences Unit, University of Cambridge, Cambridge, UK

[3]Scientific Institute, IRCCS E. Medea, Conegliano, Treviso, Italy

[4]Department of Developmental Psychology and Socialisation, University of Padua, Padua, Italy

[5]Department of Psychiatry, University of Cambridge, Cambridge, UK

Correspondence
Giovanni Mento, NeuroDev Lab, Department of General Psychology, University of Padua, Via Venezia, 8, Padua 35131, Italy.
Email: giovanni.mento@unipd.it

Abstract

The temporal dynamics of resting-state networks may represent an intrinsic functional repertoire supporting cognitive control performance across the lifespan. However, little is known about brain dynamics during the preschool period, which is a sensitive time window for cognitive control development. The fast timescale of synchronization and switching characterizing cortical network functional organization gives rise to quasi-stable patterns (i.e., brain states) that recur over time. These can be inferred at the whole-brain level using hidden Markov models (HMMs), an unsupervised machine learning technique that allows the identification of rapid oscillatory patterns at the macroscale of cortical networks. The present study used an HMM technique to investigate dynamic neural reconfigurations and their associations with behavioral (i.e., parental questionnaires) and cognitive (i.e., neuropsychological tests) measures in typically developing preschoolers (4–6 years old). We used high-density EEG to better capture the fast reconfiguration patterns of the HMM-derived metrics (i.e., switching rates, entropy rates, transition probabilities and fractional occupancies). Our results revealed that the HMM-derived metrics were reliable indices of individual neural variability and differed between boys and girls. However, only brain state transition patterns toward prefrontal and default-mode brain states, predicted differences on parental-report questionnaire scores. Overall, these findings support the importance of resting-state brain dynamics as functional scaffolds for behavior and cognition. Brain state transitions may be crucial markers of individual differences in cognitive control development in preschoolers.

Practitioner Points

- Hidden Markov model-derived metrics are reliable hallmarks of individual neural variability and show sex-related differences.
- Brain state transition patterns toward prefrontal and default-mode brain states predict differences on parental-report questionnaires scores.
- Brain state transitions may be crucial markers of individual differences in cognitive control development in preschoolers.

1 | INTRODUCTION

Resting-state brain activity can be defined as an intrinsic functional repertoire of spontaneously active fluctuations with specific spatio-temporal patterns (Baker et al., 2014). These endogenous dynamics provide the functional substrate for exogenous and/or task-evoked activations, and are related to behavioral and cognitive outcomes (Avery et al., 2020; Barnes et al., 2016; Cai et al., 2018; Jones et al., 2022; Poole et al., 2016). The brain's functional organization has largely been investigated across the lifespan using a variety of neuro-imaging techniques, such as fMRI (Smith et al., 2013; Smitha et al., 2017), MEG (Brookes et al., 2011; Wens et al., 2014) and EEG (Duma et al., 2021, 2022; Yuan et al., 2016). These studies have yielded novel insights highlighting a diffuse-to-local developmental shift in activation patterns accompanied by the strengthening of long-range connectivity at the expense of local connectivity (Fair et al., 2007; Uddin et al., 2010). Crucially, the capability of networks to dynamically modulate their functional organization stands as a scaffolding property, enabling adaptive responses to environmental demands through goal-directed forms of behavior (Bassett et al., 2006; Braun et al., 2015). Put simply, if functional networks are to be a meaningful scaffold for cognition, then they must have the capacity to organize and reorganize at a subsecond timescale. This is particularly relevant for dynamic and flexible processes subsumed under the banner of cognitive control (CC; Diamond, 2013; Braem & Egner, 2018). CC, also known as Executive Function, refers to the mental processes that enable individuals in everyday life to regulate thoughts, emotions and behaviors based on current demands and social context. It involves several key components, such as self-regulation and inhibition, working memory and cognitive flexibility (Miyake & Friedman, 2012).

However, the relationship between resting-state network (RSN) reconfiguration and CC remains unclear. Many studies suggest that CC relies on the flexible interplay between the CC network (CCN)—a distributed circuit of regions (including fronto-parietal areas)—and the default-mode network (DMN) (Alvarez & Emory, 2006; Dwyer et al., 2014; Mansouri et al., 2017; Niendam et al., 2012; Rottschy et al., 2012; Satterthwaite et al., 2013). The CCN activates in task-positive conditions (i.e., when participants are actively engaged in a task), when CC is required to achieve a goal or resolve a conflict,

whereas the DMN activates in task-negative, resting-state conditions and has been associated with self-referential processing and states of mind-wandering (Raichle, 2015). The progressive segregation between these two networks across development supports cognitive and behavioral refinement over time (Breukelaar et al., 2020). As development progresses, the energetic costs associated with transitioning toward CCN regions decrease, possibly due to structural white matter maturation (Cui et al., 2020; Tang et al., 2017).

As it has been shown that the interplay between CCN and DMN is crucial for task-related CC, their intrinsic dynamic interaction as measured during resting state may be used as a proxy for understanding CC efficiency across the lifespan (Hutchison & Morton, 2016; Kupis et al., 2021; Nomi et al., 2017). Cortical networks are characterized by a fast timescale of synchronization and switching, resulting in quasi-stable brain state patterns that recur over time (Allen et al., 2014; Liu & Duyn, 2013), which provides fundamental scaffolding for cognitive processes (Bressler & Tognoli, 2006; Brookes et al., 2014; Hutchison et al., 2013). However, the majority of studies inspecting these phenomena have used methods (e.g., sliding window approaches, clustering techniques) that do not track millisecond-scale temporal dynamics of latent brain processes (Taghia et al., 2018). Methods that are able to capture finer timescales may be necessary to investigate the dynamic nature of activity across the whole brain. Individual differences in neural dynamics might be particularly relevant during early childhood, which is a sensitive window for CC development (Diamond, 2013). During this age period, improved inhibition, flexibility and working memory are supported by functional changes in CCNs, but little is known about their underlying fine-grained dynamics. A promising computational approach that is able to track rapid oscillations within cortical networks is hidden Markov model (HMM), an unsupervised machine learning technique that allows the identification of mutually exclusive discrete patterns of whole-brain spontaneous activity that recur over time (Vidaurre et al., 2018). Importantly, HMMs allow the characterization of whole-brain transitions between discrete states of stable and coordinated activity. HMMs have been used to infer resting-state and task-related dynamic properties from a range of different neuroimaging techniques, such as fMRI (Dang et al., 2017; Goucher-Lambert & McComb, 2019; Hussain et al., 2023), MEG (Baker et al., 2014; Hawkins et al., 2020; Quinn et al., 2018; Vidaurre et al., 2018) and EEG (Dash et al., 2020;

Marzetti, 2023; Obermaier et al., 2001; Williams et al., 2018). Previous studies have revealed that the dynamic properties of RSNs are related to a variety of cognitive and behavioral outcomes (Cabral et al., 2017; Taghia et al., 2018; Vidaurre et al., 2017). Interestingly, neural dynamics may be related to individual differences across neurodevelopment, including neurodevelopmental conditions like attention-deficit hyperactivity disorder (ADHD) and autism (Dammu & Bapi, 2019; Maya Piedrahita, 2021; Scofield et al., 2019). However, the majority of studies that have inferred HMMs from neuroimaging data have only included adult participants, and there has been a relatively limited focus on childhood development. A recent study used HMMs to investigate spontaneous neural dynamics in a transdiagnostic sample of 8–13 year old children (Zdorovtsova et al., 2023) and revealed a positive association between the complexity of individuals' transitions (i.e., entropy) among RSNs and general cognitive ability (as measured using the Wechsler Abbreviated Scales of Intelligence II—Matrix Reasoning Subtest). Additionally, the specific pattern of between-state transitions and time spent in each state further explained individual variations in cognitive ability: transitioning into or spending time within DMN-like and fronto-parietal/sensory states was associated with decreased and increased cognitive ability, respectively. Examining the fine-grained dynamics of RSNs at different developmental timepoints may yield further insights into how the relationships between neural dynamics, cognition, and behavior change throughout early life.

Given the importance of the preschool-age period for CC development, the present study investigated the relationships between neural dynamics and measures of cognition and behavior in a sample of preschool-aged children (4–6 years). We used high-density EEG (hdEEG) to better capture fast reconfiguration patterns of HMM-derived metrics. These included switching rates (SRs; i.e., rate of switching between brain states), entropy rates (i.e., complexity of individuals' transitions), transition probabilities (i.e., the probability of switching from each brain state to all the others) and fractional occupancies (i.e., the overall proportion of time spent in each state).

As a first step, we checked the within-subject reliability of our HMM-derived metrics. This holds significant importance in assessing the validity of these metrics before correlating them with behavior and cognition. For this purpose, we recorded hdEEG during two separate resting-state sessions per subject, from which we derived HMM-based indices. The brain states allocation was purposely performed over the EEG-derived source activation. In fact, we aimed at characterizing the spatial configuration of functional organization patterns of cortical dynamics, allowing inference regarding co-activations across brain regions (Ding et al., 2022; Eickhoff et al., 2011). Additionally, source-based connectivity provides more accurate and localized measures of brain activity compared to scalp-based methods, as it mitigates the effects of volume conduction and reference choice, leading to improved interpretation of neural interactions (Hauk, 2004; Michel & Murray, 2012). Moreover, we assessed the effect of age and sex on these indices as prior studies suggested that both these factors may impact brain dynamics in older populations (Kupis et al., 2021; Scofield et al., 2019). Then, as the main goal we investigated the
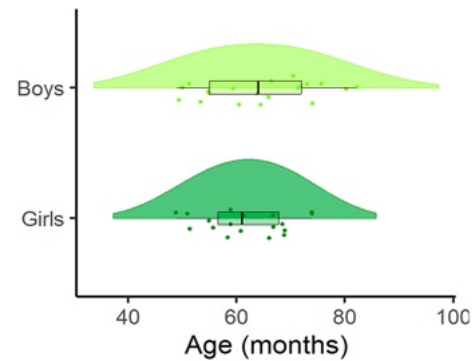
FIGURE 1 Raincloud plot depicting the distribution of age (months) across boys (light green) and girls (dark green). The box plots represent the interquartile range (IQR) with the median marked by a vertical bold line. The "cloud" portions display the probability density of the data, providing insights into its distribution. Each data point is also shown to highlight individual observations.

relationship between HMM-derived indices with broader measures of behavior (parental questionnaires) and cognition (cognitive tests assessing non-verbal reasoning, verbal working memory, self-regulation and inhibition). Again, previous studies present divergent findings; some indicate positive associations (Taghia et al., 2018; Zdorovtsova et al., 2023) while others report negative relationships (Cabral et al., 2017) between SRs and cognitive performance. We expected positive relationships between CCN-like state transitions, fractional occupancies and cognitive ability, and negative associations between DMN-like state indices and cognitive ability (Zdorovtsova et al., 2023).

2 | MATERIALS AND METHODS

2.1 | Participants

Fifty-nine participants were initially enrolled. Children (4–6 years old) were recruited from a local kindergarten in the Venetian Region of Italy. Nonverbal reasoning was assessed using the colored progressive matrices (CPMs; Raven & Court, 1938) and children with a CPM score 2 or more standard deviations below the population mean were excluded ($N = 1$). Moreover, we excluded children for whom at least one of the two at-rest hdEEG recording sessions was discarded due to excessive noise/movement artifacts ($N = 19$). Participants had no known or diagnosed sensory, neurological or neuropsychiatric disorders and normal or corrected-to-normal vision. The final sample included 39 children (18 girls; 4–6 years, M = 4.8; sd = 0.7). The demographic characteristics of the sample are described in Figure 1.

2.2 | Ethics statement

Children's parents provided written consent for their children's participation. All experimental procedures were approved by the Ethics

Committee of the School of Psychology of the University of Padua (protocol No. 4751) and were conducted according to the principles expressed in the Declaration of Helsinki.

2.3 | Experimental procedure

Children and their families were welcomed to the University's hdEEG lab. Children were given time to familiarize themselves with the environment and with the experimenters while all experimental procedures were explained to parents, who provided written consent for their children's participation. After assessing children's oral assent to participate in the activities, an hdEEG 128-channel sensor net was applied.

The protocol included three main activities in the following order: (1) resting-state session 1 (7 min), (2) resting-state session 2 (7 min), and (3) neuropsychological tests (~10 min). Between each activity, children watched ~5 min of an entertaining cartoon (The House of Mickey Mouse, Walt Disney). In the meantime, parents filled in a series of questionnaires assessing children's behavioral and emotional profiles. Parental questionnaires were administered through the online platform *Qualtrics Survey* (Qualtrics, n.d., Provo, UT).

2.4 | Cognitive measures

Nonverbal reasoning was assessed using the CPMs, in which children are required to complete a series of geometrical patterns and shapes (CPM, series A, B, AB; Raven & Court, 1938). Moreover, in order to obtain a wide descriptive profile of children's CC abilities, we collected both neuropsychological measures (see Table 1) and parental questionnaires assessing everyday behavior, executive functioning, and emotion regulation (see Table 2).

2.4.1 | Neuropsychological measures

Phonological fluency was assessed as a measure of lexical access based on phonological cues and required children to say all the words

TABLE 1 Cognitive tests. Here, we report *means, standard deviations* and *range values* calculated for the neuropsychological tests across our sample. To derive a measure of phonological fluency, we calculated the mean number of words per category (total number of words/number of categories) per participant; for gift wrap and gift time, we calculated the total time in seconds per participant. The sample's scores were within the Italian normative range in all the reported measures.

Test	Score mean ± sd (range)
Colored progressive matrices	20.0 ± 5.0 (10–34)
Phonological fluency	2.3 ± 1.5 (0.7–7.3)
Backward digit span	2.1 ± 1.2 (0–4)
Gift wrap (time in s)	46.9 ± 18.0 (1–60)
Gift wait (time in s)	98.6 ± 99.2 (0–240)

they knew starting with a specific letter in 1 min (BVN 5–11, Bisiacchi et al., 2005). Backward digit span (BDS) was assessed as a measure of verbal working memory and required children to retrieve a series of numbers in reverse order (BVN 5–11, Bisiacchi et al., 2005). Finally, gift wrap and gift wait (FE-PS 2–6, Usai et al., 2017) were administered to assess children's levels of self-regulation and inhibition. Here, children were asked to wait with their eyes closed while the experimenter was wrapping a gift for them (total duration 1 min); afterward, the wrapped gift was placed in front of them and they were told that they could open it, but the longer they waited before opening (maximum waiting time 4 min), the bigger the gift would be.

2.4.2 | Behavioral questionnaires

The behavioral and emotional profile of children was assessed using the Conners revised scales for parents (CPRS; Conners et al., 1998; Italian adaptation by Nobile et al., 2007), a parental questionnaire that comprises a series of statements about children's behavior in everyday life. Children's executive functioning in ecological contexts (e.g., home) was assessed using the Behavior Rating Inventory of Executive Function Preschool version (BRIEF-P; Gioia et al., 1996; Italian adaptation by Marano et al., 2014), a parental questionnaire

TABLE 2 Parental questionnaire scores. Here, we report *means, standard deviations*, and *range values* calculated for the parental questionnaires across our sample. For each questionnaire, only total scales (highlighted in bold) entered subsequent statistical analyses. The sample's scores were within the Italian normative range in all the reported questionnaires' subscales.

Test	Score mean ± sd (range)
Conners (Oppositivity)	2.1 ± 1.3 (0–5)
Conners (Cognitive problems and disattention)	4.5 ± 2.3 (0–9)
Conners (Hyperactivity)	3.4 ± 2.2 (0–10)
Conners (Anxiety and shyness)	2.4 ± 1.5 (0–6)
Conners (Perfectionism)	2.4 ± 2.1 (0–8)
Conners (Social problems)	2.1 ± 1.5 (0–6)
Conners (Psychosomatic problems)	0.2 ± 0.7 (0–4)
Conners (ADHD index)	3.4 ± 3.1 (0–12)
Conners (DSM-IV total scale)	**9.6 ± 5.3 (0–19)**
BRIEF (Inhibition)	21.8 ± 3.3 (16–28)
BRIEF (Shifting)	12.5 ± 2.6 (10–21)
BRIEF (Emotion regulation)	13.9 ± 2.3 (10–18)
BRIEF (Working memory)	21.0 ± 3.8 (17–31)
BRIEF (Planification-organization)	13.7 ± 2.1 (11–19)
BRIEF (Global Executive Composite)	**82.8 ± 9.5 (69–111)**
ERC (Emotional regulation)	27.0 ± 5.6 (0–32)
ERC (Lability/negativity)	53.7 ± 9.7 (0–62)
ERC (total scale)	**80.7 ± 14.8 (0–94)**
IUS-C (total scale)	**23.3 ± 8.1 (0–42)**

that comprises a series of statements about children's executive functioning in everyday life. Children's emotion regulation was assessed using the Emotion Regulation CheckList (ERC; Molina et al., 2014), a parental questionnaire that comprises a series of statements assessing emotionality and regulation in children (e.g., affective lability, intensity). Finally, the Intolerance of Uncertainty scale for children (IUS-C, Comer et al., 2009; Italian adaptation by Bottesi et al., in prep.) was administered as a measure of cognitive adaptability in unpredictable contexts. Indeed, this parental questionnaire assesses the dispositional inability to tolerate the aversive reactions triggered by a perceived lack of sufficient and/or salient information.

2.5 | hdEEG recording

The high spatial resolution EEG signal was recorded through a 128-channel Geodesic hdEEG System (EGI GES-300), with electrical reference to the vertex. A sampling rate of 500 Hz was used and impedance was kept below 60 kΩ for each electrode. Preprocessing was performed through EEGLAB v2022.0 (Delorme & Makeig, 2004).

Importantly, hdEEG was recorded during a resting-state session with eyes-open. Meanwhile, children watched the abstract video Inscapes, which was purposely designed to improve compliance while minimizing motion and cognitive load during neural data acquisition (Vanderwal et al., 2015). We only recorded eyes-open resting-state EEG activity to avoid an excessive data drop out given the young age of participants. To note, previous studies revealed substantial differences in fMRI- but not in EEG-derived brain states metrics between eyes-open and eyes-closed resting state (Ingram et al., 2024).

3 | DATA ANALYSIS

3.1 | hdEEG source reconstruction

3.1.1 | Preprocessing and co-registration

The continuous EEG signal was first downsampled at 250 Hz and then band-pass-filtered (1–30 Hz) using a Hamming windowed-sinc finite impulse response filter. After filtering, the continuous EEG was visually inspected and bad segments (e.g., gross motor artifacts) were manually removed. Independent component analysis (ICA; Stone, 2002) using the Infomax algorithm (Bell & Sejnowski, 1995) was used to perform data cleaning. Independent components were visually inspected in topography and time-series, and those clearly related to eye blinks, eye movements, muscle artifacts, and heartbeat were discarded. The remaining components were then projected back to the electrode space to obtain a cleaner EEG signal. Finally, flat and bad channels were reconstructed with the spherical spline interpolation method (Perrin et al., 1989). The data were then rereferenced to the average of all electrodes. Participants' hdEEG data were co-registered using a natural (asymmetric) NIHPD Objective 1 scan template intended for preschool-aged children (4.5–8.5 years; Fonov

et al., 2011). Co-registration was performed using the digitized scalp locations and fiducial markers using an iterative closest point algorithm in SPM12 (Ashburner et al., 2014). A forward model was fitted using the boundary element method (Hall & Hall, 1994).

3.1.2 | Source-localization and parcellation

Final preprocessing steps were implemented using the OHBA Software Library (OSL v2.0.3; Oxford Centre for Human Brain Activity [OHBA] Analysis Group, 2017) and OHBA's HMM Library (HMM-MAR; Vidaurre et al., 2016). First, a covariance matrix was computed across the whole-time course for each participant and PCA rank reduction allowed regularization of the obtained matrix to 50 dimensions. Then, a linearly constrained minimum variance beamformer was used to estimate whole-brain source-space activity for points in an 8 mm grid (Van Veen et al., 1997). Data dimensionality was reduced so that each individual brain activity was estimated as a series of time-courses for 3559 source locations across the brain using signal-space separation algorithm (Woolrich et al., 2011). Afterward, hdEEG data were further reduced into a 38-node cortical parcellation following the method proposed in Quinn et al. (2018). Finally, the parcellation was binarized to estimate a single time-course per node from the first principal components across voxels; crucially, this resulted in the reduction of individual time-courses to 38 parcels instead of 3559 voxels, enabling additional corrections for signal leakage.

3.1.3 | Additional preprocessing steps

Following OHBA's HMM-MAR library, additional preprocessing steps were taken prior to the HMM initialization: detrending, signal standardization, and corrections for signal leakage. First, detrending removed linear trends in the data for each channel separately; second, participants' concatenated time-courses were standardized. Next, signal leakage introduced by source reconstruction with zero temporal lag was corrected using multivariate orthogonalization (Colclough et al., 2015). Then, the Hilbert transform allowed absolute signal amplitude estimation for each source at each timepoint (see Figure 2 for a visual schematic representation of the preprocessing procedure).

3.2 | Hidden Markov modeling

In the present study, we used the HMM-MAR toolbox (Vidaurre et al., 2016), developed by the OHBA to infer an HMM from resting-state hdEEG time-series data. HMM refer to a set of unsupervised machine learning techniques that allow the segmentation of observed time-series data into a set of discrete hidden functional states (HMM states). These HMM states recur over millisecond timescales and are mutually exclusive in time. A single model infers HMM states assuming they all have the same probabilistic distributions but with different parameterizations (Figure 2). In the present study, we employed the
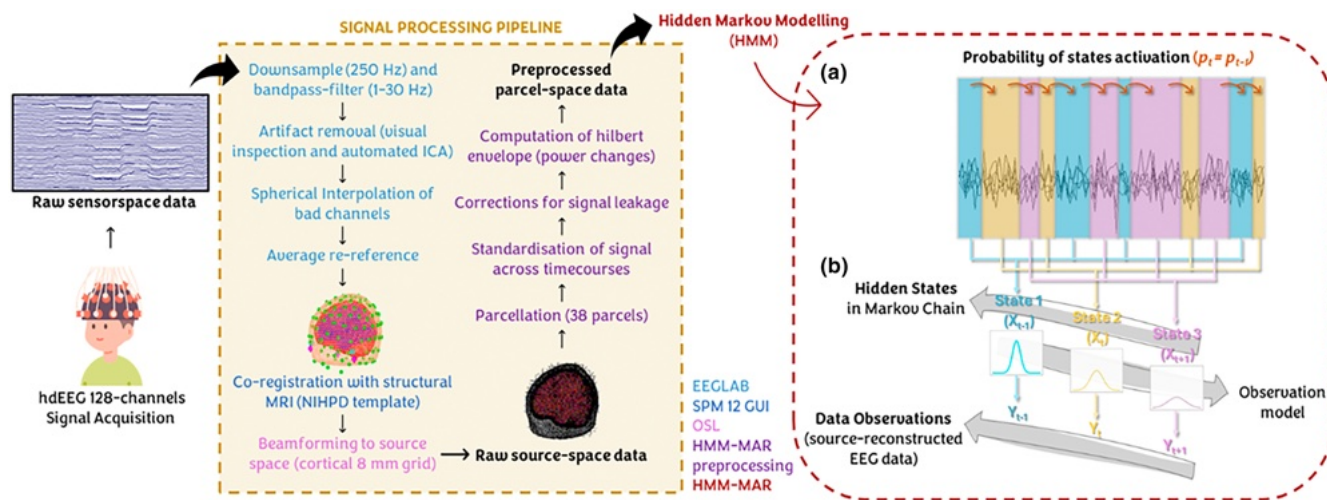
FIGURE 2 Data preprocessing pipeline and graphical representation of the HMM. On the left is a visual representation of each step of our hdEEG data preprocessing pipeline, in addition to the software packages and toolboxes used to complete each step of the pipeline. On the right is presented the HMM: (a) the basic principle assumes that a time-series can be described using a hidden sequence of a finite number of states. Here, the time-series is partitioned into three states denoted by the blue, yellow and pink slabs. The model assumes that the probability (p) of each state at time point t depends on which state was active at time point $t − 1$, as represented by the brown arrows. (b) The model then assumes that the data observed in each state are drawn from a probabilistic observation model.

same formal definitions as in Zdorovtsova et al. (2023) (see Supplementary Section 1). Importantly, the aim was to investigate whether differences in behavioral and cognitive measures can be tracked by a parsimonious number of brain states. Given that HMM computation requires an a priori specification of the number of states (k), we exploratory run separate HMMs with prespecified states (i.e., $k = 4$ to $k = 10$). After visual inspection, we selected the solution revealing distinct spatiotemporal activity patterns while mitigating the redundancy associated with higher-state solutions. To note, in the current study, we did not use free energy metrics. Indeed, even if they allow an objective basis for selecting the number of states (i.e., the lower the free energy, the better the k solution), it is debatable whether it truly promotes parsimony and theoretical coherence. In this regard, free energy often increases monotonically up to 15 states, implying that a Bayes-optimal solution would need an even higher number of states (Baker et al., 2014). Similarly, when using traditional dimensionality reduction techniques (e.g., ICA), fewer predefined components typically identifies canonical RSNs, while using more components can only reveal finer distinctions in activity patterns (Smith et al., 2011; Smitha et al., 2017).

The HMM-MAR toolbox computes a range of outputs that are useful in estimating different HMM states' features. First, each state's temporal characteristics were quantified in terms of state fractional occupancies (i.e., the fraction of the total time spent in a state). Second, a SR (i.e., the frequency of state switching across an individual time-course) was calculated for each participant, providing a measure of individual network stability. The joint probabilities of transitions between pairs of states contained in the HMM output also allowed to compute state transition probability matrices for each participant, as well as for the entire concatenated time-course. Moreover, these allowed us to calculate an entropy rate estimate (i.e., a measure of

average uncertainty generated by a transition within a sequence) per participant following the method employed by Zdorovtsova et al. (2023).

To note, we run HMM on both resting-state sessions together in order to (1) get more data and derive more representative states and (2) get the possibility to correlate the two recordings. This could not have been achieved if running two HMM separately per resting-state session, as we would have lost the identical correspondence between brain states. All subsequent analyses were performed on the HMM-metrics of the first resting-state session, as this was prior to our experimental session and should be considered the baseline (although we report the same analyses on the HMM-metrics averaged across the two resting-state sessions in the Supplementary Section 7).

3.3 | Statistical analysis

Here, we provide a brief description of our research questions and the analyses we conducted to address them. Statistical analysis was performed using R (R Core Team, 2021; version 4.3.2). A Bayesian framework was used when fitting linear, generalized or multivariate linear models (R package: "brms"; Bürkner, 2017). Models' specifications (i.e., number of chains, samples, burn-in, family distribution, custom, or default priors) are specified in the supplementary materials. Convergence was assessed by examining the R-hat values (with a maximum accepted value for satisfactory convergence of 1.05 as suggested by Vehtari, Gelman, Simpson, et al., 2021), and by visual inspection of traces and the posterior predictive check. We employed leave-one out cross-validation to evaluate the model performance and identify potential influential observations using k-Pareto diagnostics (R package: "loo"; Vehtari, Gelman, Gabry, & Yao, 2021). Based on the

k-Pareto diagnostic plot, we considered observations with a Pareto shape parameter exceeding 0.7 as potentially influential. For each model, we report the estimated parameter value β, with an 89% highest density interval (HDI) [lower limit, upper limit]. The use of an 89% HDI provides a narrower interval compared to traditional 95% intervals, thus allowing for a more focused estimate while still maintaining a high level of confidence. This choice of interval reflects a balance between precision and robustness in our inference (Makowski et al., 2019). Moreover, we report standardized betas (βs), computed as the ratio of the unstandardized beta coefficient to the standard deviation of the predictor variable (sigma), in order to offer a consistent measure of the relative impact of predictors on the outcome.

For hypothesis testing, we used the region of practical equivalence (ROPE; Kruschke, 2018; R package: "bayestestR," Makowski et al., 2019). The ROPE is defined as a region corresponding to the null value and the bulk of the posterior of a given parameter is compared with this region of values. If the HDI is completely outside the ROPE, the null hypothesis is "rejected," while if the HDI overlaps with the ROPE the null hypothesis is "accepted." For descriptive purposes, we consider less than 5% strong evidence of a relevant effect. We would like to point out that our observed variables are often very small, on a scale of thousandths; consequently, ROPE ranges tend to be generally narrow.

3.4 | Individual neural variability

First, two linear models were fitted separately for SR and entropy rates (see Supplementary Table S1); specifically, each model comprised values of SR (standardized) or entropy (standardized) during the second resting-state session as dependent variables and the values of SR or entropy during the first resting-state session as independent variables. The models included a total of 39 observations (see Supplementary Sections 2.1 and 2.2 for models' specifications). Here, we used an ROPE range = [−0.2, 0.2] for equivalence testing.

Second, for fractional occupancies (N° states × N°subjects) and state transition probabilities (N°states^2 × N°subjects) we computed both within- and between-subjects Spearman correlations across the two resting-state sessions. For both fractional occupancies and state transition probabilities, within-subjects correlations were computed as the correlation of each subjects' measures between resting state 1 and resting state 2 (i.e., for each subject, 6 × 6 fractional occupancies and 36 × 36 transition probabilities; output = N°subjects × 1 correlation coefficient). Between-subjects correlations were computed as the correlation of each subject's measures with the measures of each other subject at resting state 2 (i.e., for each subject, 6 × 6 × (N°subjects-1) fractional occupancies and 36 × 36 × (N°subjects-1) transition probabilities; output = N°subjects × (N°subjects-1) correlation coefficients). Afterward, two separated generalized linear models were fitted for fractional occupancy and transition probabilities (see Supplementary Table S1) with Spearman's correlation coefficients as dependent variables, the type of correlation (within vs. between) as independent variables and with a random intercept per subject.

The model included a total of N°subjects × within correlation (one per subject) + N°subjects × between correlation (38 per subject) (see Supplementary Sections 2.3 and 2.4 for model specifications). Here, we used an ROPE range = [−0.01, 0.01] for equivalence testing.

3.5 | Age- and sex-related differences

In the following analysis, we evaluated the effect of age (standardized, in months) and sex on the HMM indices computed for the first set of resting-state recordings: (1) SR, (2) entropy rates, (3) states' fractional occupancies, and (4) probabilities of transitioning into each state (i.e., computed as the mean of transition probabilities toward each state, excluding self-transitions: all transition probabilities toward the same state were averaged). This latter measure reduced data dimensionality (from 36 to 6 transitions) and allowed us to formulate more precise hypotheses. We fitted two separate linear models for SR and entropy rates and one multivariate linear model for transition probabilities. For fractional occupancies, we run separate linear models for each state (see Supplementary Table S2). The models included a total of 39 observations. Here, we used a default ROPE range for equivalence testing (see Supplementary Sections 3.1–3.4 for models' specification).

3.6 | Individual neural variability and CC

In the following analysis, for each subject we used HMM indices computed for the first set of resting-state recordings (see above). To assess the relationship between cognitive and behavioral measures with HMM-derived indices, we fitted two multivariate linear models for each HMM index (each index was standardized) entering as dependent variables either (1) neuropsychological (NPS) measures (i.e., phonological fluency mean score, Gift wrap time and CPM score) or (2) questionnaires total scales (i.e., CPRS DSM-IV, BRIEF Global Executive Composite [GEC], ERC, and IUS). BDS and Gift wait were excluded from NPS models due to their non-normal distribution in order to maintain the assumption of normality necessary for reliable estimation. Age (standardized, in months) and sex entered as covariates in all the models (see Supplementary Table S7). NPS models included a total of 39 observations, questionnaires' models included a total of 38 observations due to missing data for one participant. Here, we used a default ROPE range for equivalence testing (see Supplementary Sections 4.1 and 4.2 for models' specification).

4 | RESULTS

4.1 | State characteristics for the six-state HMM

A six-state HMM solution was selected as it revealed distinct spatio-temporal activity patterns while mitigating the redundancy associated with higher-state solutions (Figure 3; see Supplementary Figure S1 for
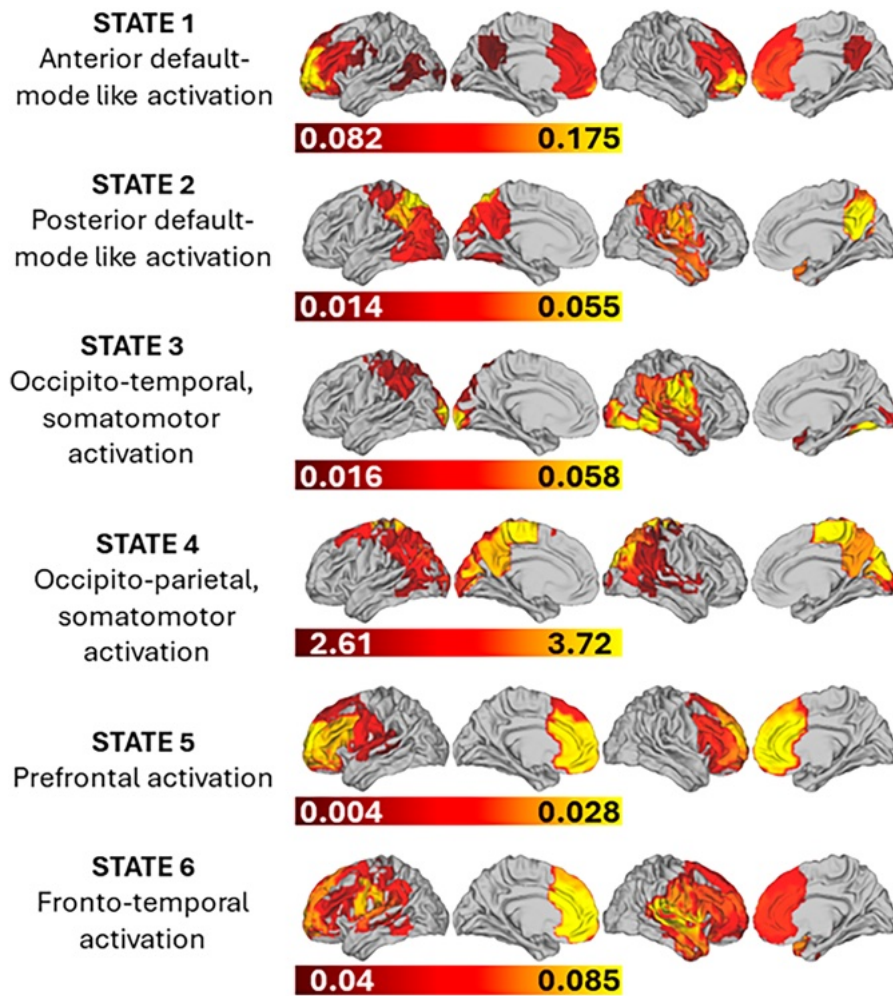
FIGURE 3 Six-state HMM. Here, we present the visual representations of the six-state HMM. For each state, the top 60% of positive activations were plotted on a cortical surface using the HCP Workbench GUI. State labels correspond to our descriptions of the macroscopic features of the cortical activation pattern.
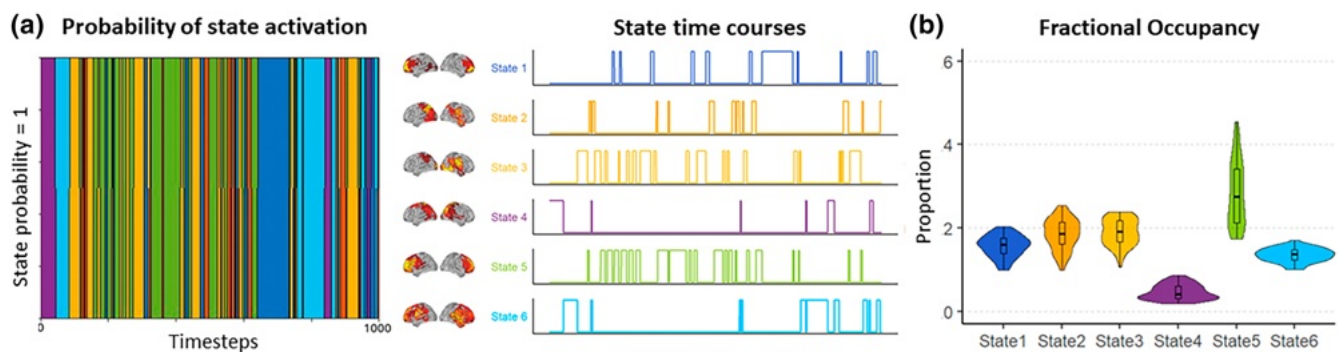
FIGURE 4 Temporal characteristics of the HMM states during both resting-state sessions. (a) The first 1000 timesteps (4 s sampled at 250 Hz) of the Viterbi path (i.e., maximum a posteriori sequence of states in an HMM) and state time courses are presented. (b) Fractional occupancy (FO) of the states in our $k = 6$ HMM.

parcel activation). Each state-map displays the average activation profile of each parcel for the concatenated hdEEG dataset (for each subject, resting state 1 and resting state 2). State-specific activations are plotted as yellow/red. State 1 involves activations over prefrontal and temporo-parietal areas, resembling a prominent anterior DMN-like state. State 2 involves a lateralized pattern of activation in temporo-parietal regions of the cortex including the precuneus, and

can be configured as a posterior DMN-like state. State 3 and 4 involve posterior regions including somatomotor areas and, respectively, occipito-temporal and occipito-parietal areas. Finally, state 5 and 6 display, respectively, prominent prefrontal and fronto-temporal activations.

Temporal features of each HMM state were derived from state time-courses (Figure 4). In terms of fractional occupancies (FO;

i.e., the total average time spent in each state), state 4 displays the lowest FO and state 5 the greatest variability. Means and standard deviations of LTs, ITs, and FOs are summarized in Table 3.

Finally, state transition probabilities between and across participants were computed. The dominant type of timepoint-to-timepoint transition was "self-transition," forming the diagonal of the state transition probability matrix. Therefore, the diagonal was zeroed out to visualize state-to-state transition probabilities (Figure 5).

4.2 | Individual SR, entropy, fractional occupancies, and brain state transitions are reliable hallmarks of individual neural variability

To assess whether SR, entropy rates, fractional occupancies and brain state transitions are reliable hallmarks of individual neural

variability, we ran separate linear and generalized linear models (see Supplementary Table S1). For SR (see Supplementary Table S1, 1_M1), the estimated regression coefficient (β) was .82 (89% HDI: [0.68, 0.98], βs = 1.46) and the percentage of β inside the ROPE was smaller than 5% (i.e., <1%). Similarly, for entropy (see Supplementary Table S1, 1_M2), the estimated regression coefficient (β) was .82 (89% HDI: [0.66, 0.97], βs = 1.49) and the percentage of β inside the ROPE was less than 5% (i.e., <1%). Therefore, we concluded that both SR and entropy rates correlated between the two resting-state sessions, suggesting that the dynamics of these states are relatively stable measures of individual differences.

For fractional occupancies (see Supplementary Table S1, 1_M3), the estimated regression coefficient (β) was .08 (89% HDI: [0.04, 0.12], βs = .53) and the percentage of β inside the ROPE was less than 5% (i.e., <1%). Regarding transition probabilities (see Supplementary Table S1, 1_M4), before computing within- and between-subjects Spearman correlations, for computational reasons we removed low-probability transitions ($<1 \times 10^{-5}$) ($N = 4$, S2 → S4, S2 → S9, S3 → S1, S3 → S6). Indeed, nonzero variability is required to calculate correlations accurately. The estimated regression coefficient (β) was .03 (89% HDI: [0.02, 0.04], βs = .75) and the percentage of β inside the ROPE was less than 5% (i.e., <1%). Therefore, for both fractional occupancies and transition probabilities, results indicate greater correlation coefficients in the within-subjects compared to the between-subjects correlations (see Figure 6 for visual representation of the results).

Overall, these results confirm within-subjects correlation of HMM-derived indices (i.e., SR, entropy rates, fractional occupancies, and transition probabilities), supporting these as reliable hallmarks of individual neural variability.
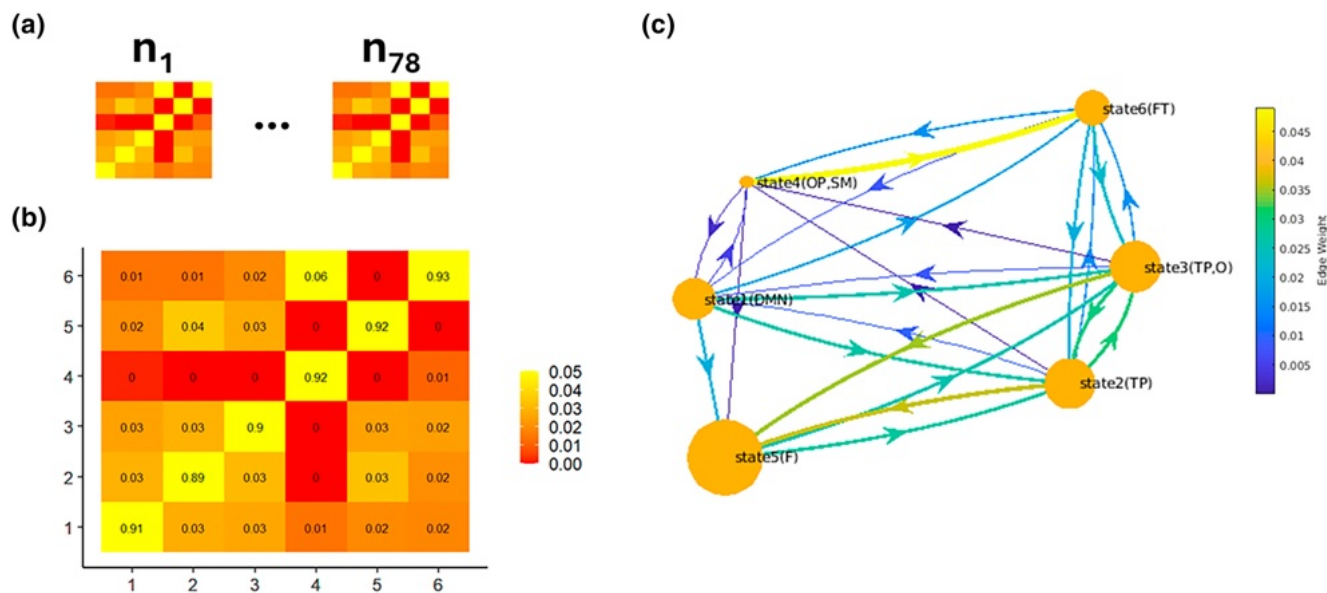
TABLE 3 Means and standard deviations for state fractional occupancy during both resting-state sessions. Note that no thresholding was applied in the calculation of these metrics.

State	Fractional occupancy (proportion) mean ± sd
State 1 (anterior DMN like)	0.157 ± 0.026
State 2 (posterior DMN like)	0.187 ± 0.037
State 3 (OT, SM)	0.190 ± 0.032
State 4 (OP, SM)	0.047 ± 0.018
State 5 (PF)	0.284 ± 0.077
State 6 (FT)	0.136 ± 0.016

FIGURE 5 (a) Joint posterior probabilities of state transitions for each subject were computed. (b, c) Average transition probabilities across the entire sample during both resting-state sessions ($n = 78$). Self-transitions were intentionally excluded for the purpose of plotting state-to-state transitions. No thresholds were applied. The node sizes in (c) reflect each state's fractional occupancy.
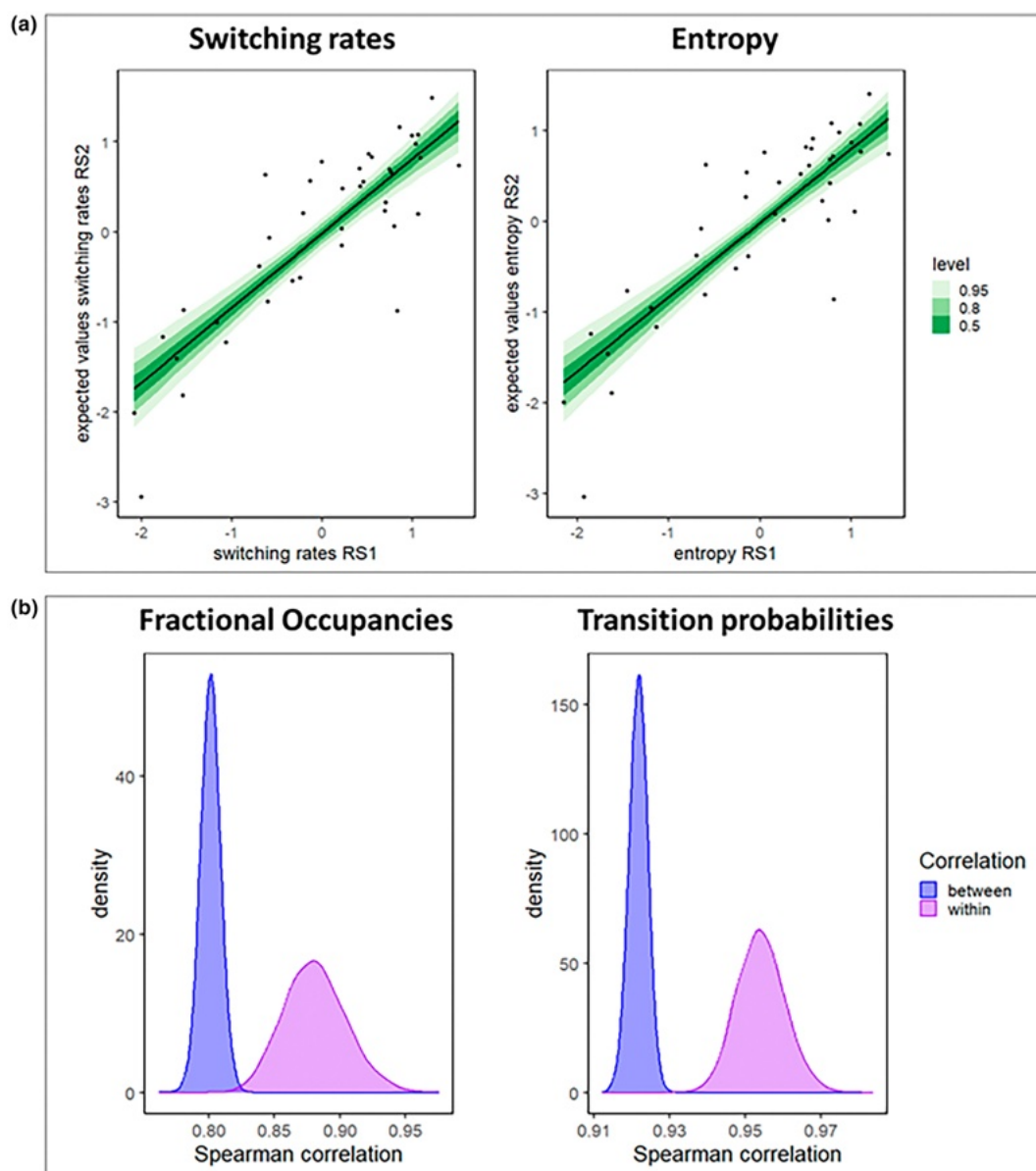
FIGURE 6 Panel (a): The two figures display SR (left) and entropy (right) correlations between the two resting-state sessions. On the X-axis are displayed expected values of SR/entropy in the first resting-state session (RS1), on the Y-axis are displayed expected values of SR/entropy in the second resting-state session (RS2). Panel (b): The two figures display, for fractional occupancies (left) and transition probabilities (right), posterior density distributions (Y-axis) of Spearman's correlation coefficients between the two resting-state sessions (X-axis) for within (purple) and between (blue) correlations.

4.3 | Individual neural variability differs between boys and girls

To assess the effects of age and sex on HMM-derived individual neural variability indices we used separate linear and multivariate linear models (see Supplementary Table S2). For both SR (see Supplementary Table S2, 2_M1) and entropy rates (see Supplementary Table S2, 2_M2), we found a main effect of sex, with boys displaying overall higher rates than girls (respectively, $\beta = .01$, 89% HDI: [0.00, 0.01], % inside ROPE <1%, βs = 1 and $\beta = .13$, 89% HDI: [0.02, 0.23], % inside ROPE <1%, βs = .65). Regarding transition probabilities (see

Supplementary Table S2, 2_M3), we found that boys have higher probability of switching into state 2 ($\beta = .002$, 89% HDI: [0.000, 0.005], % inside ROPE <3%, βs = .5) and a lower probability of switching into state 5 ($\beta = -.003$, 89% HDI: [−0.005, −0.000], % inside ROPE <1%, βs = −.6) compared to girls. Regarding fractional occupancies (see Supplementary Table S2, 2_M4–2_M9), we found a main effect of sex in all the states, with boys spending overall more time in state 1 ($\beta = .02$, 89% HDI: [0.00, 0.03], % inside ROPE <1%, βs = 1), state 2 ($\beta = .02$, 89% HDI: [0.01, 0.04], % inside ROPE <1%, βs = .5), state 3 ($\beta = .03$, 89% HDI: [0.01, 0.05], % inside ROPE <1%, βs = 1) and state 6 ($\beta = .02$, 89% HDI: [0.01, 0.02], % inside ROPE
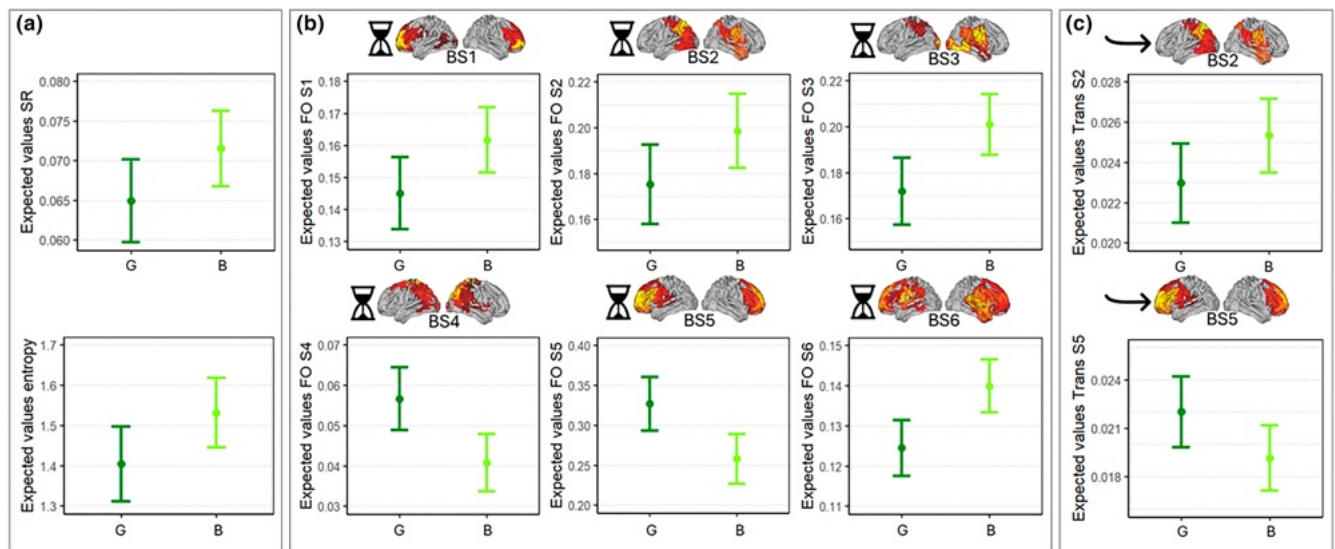
FIGURE 7 Sex-related differences in the HMM-derived indices. Panel (a): The figures show on the y-axis expected values of SR (upper figure) and entropy (lower figure) rates, in boys (B; light green) and girls (G; dark green). Panel (b): The figures show on the y-axis expected values of fractional occupancy (indicated symbolically by the hourglass) in brain state 1 (upper left), brain state 2 (upper center), brain state 3 (upper right), brain state 4 (bottom left), brain state 5 (bottom center) and brain state 6 (bottom right), in boys (B; light green) and girls (G; dark green). Panel (c): The figures show on the y-axis expected values of transition probabilities (indicated symbolically by an arrow) of switching toward brain state 2 (upper figure) and state 5 (bottom figure), in boys (B; light green) and girls (G; dark green).

<1%, $\beta s = 2$), and girls spending more time in state 4 ($\beta = -.02$, 89% HDI: $[-0.02, -0.01]$, % inside ROPE <1%, $\beta s = -1$) and state 5 ($\beta = -.07$, 89% HDI: $[-0.11, -0.03]$, % inside ROPE <1%, $\beta s = -1$). See Supplementary Tables S3–S6 for all the results, and Figure 7 for visual representation of the reported results. Overall, these results suggest the presence of sex-based but not age-based differences in individual neural variability, at least within this relatively narrow age band.

## 4.4 | Brain state transitions are related to preschoolers' CC

To unravel the relationship between individual neural variability and CC we used separate multivariate models (see Supplementary Table S7). For transition probabilities (see Supplementary Table S7, 3_M8), we found that transitioning into brain state 2 is generally associated with worse behavioral and emotional profiles on the parental questionnaires: reduced ERC scores ($\beta = -3.29$, 89% HDI: $[-5.96, -0.65]$, % inside ROPE <1%, $\beta s = -.57$), increased BRIEF-P GEC scores ($\beta = 5.78$, 89% HDI: $[1.52, 9.76]$, % inside ROPE <1%, $\beta s = .65$) and increased Conners DSM-IV total scale (CPRS DSM-IV) scores ($\beta = 3.82$, 89% HDI: $[1.51, 6.12]$, % inside ROPE <1%, $\beta s = .79$). Conversely, transitioning into brain state 3 was associated with better emotional regulation profiles as indicated by increased ERC scores ($\beta = 3.01$, 89% HDI: $[0.53, 5.55]$, % inside ROPE <1%, $\beta s = .53$), and transitioning into brain state 6 was associated with better emotional regulation and behavioral profiles as indicated by increased ERC scores ($\beta = 2.83$, 89% HDI: $[0.98, 4.81]$, % inside ROPE <1%,

$\beta s = .49$), reduced GEC ($\beta = -2.91$, 89% HDI: $[-5.73, -0.01]$, % inside ROPE <10%, $\beta s = -.33$) and CPRS DSM ($\beta = -2.07$, 89% HDI: $[-3.68, -0.43]$, % inside ROPE <2%, $\beta s = -.43$) scores. Fractional occupancies (see Supplementary Table S7, 3_M7), SR (see Supplementary Table S7, 3_M5), and entropy rates (see Supplementary Table S7, 3_M6) did not predict differences on any of the questionnaires' scales (see Supplementary Tables S8–S11 for all the results, and Figure 8 for visual representation of the reported results). Finally, none of the individual neural variability indices predicted NPS measures (see Supplementary Table S7, 3_M1–3_M4; see Supplementary Tables S12–S15 for all the results).

Overall, results only partly confirm that transitioning toward CCN-like states predicts better behavioral and emotional regulation profiles as assessed using parental questionnaires. Importantly, these results do not depend on baseline differences between boys and girls on neuropsychological measures (see Supplementary Section 9).

5 | DISCUSSION

In the present study, we investigated preschoolers' resting-state neural dynamics by inferring a six-state HMM from hdEEG data. Our model identified discrete spatiotemporal patterns mimicking well-known RSNs, including the anterior and posterior default-mode, temporo-parietal, occipital, sensorimotor, frontal, and fronto-temporal networks. The states were characterized by short (<150 ms) time courses, supporting the idea of RSNs as a system of rapid synchronization and switching dynamics. Individual SR, entropy rates, fractional occupancies and state transition probabilities were reliable across
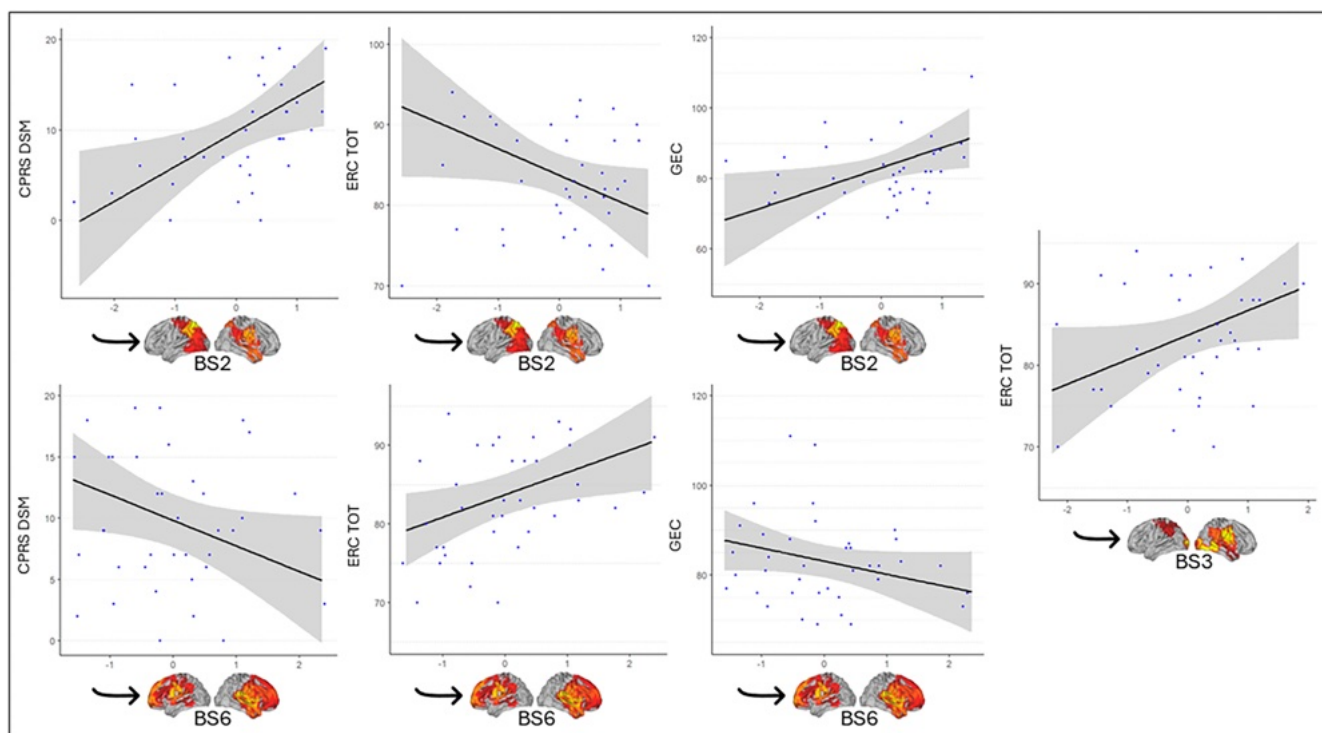
FIGURE 8 Transitions toward each state and questionnaire scores. The figures reported in the panel show on x-axis the expected values (standardized) of brain state transitions (indicated symbolically by an arrow) toward a certain brain state (i.e., BS2 = brain state 2, BS3 = brain state 3, BS6 = brain state 6) and on the y-axis the expected values of the questionnaires' scales (GEC = global executive composite [BRIEF-P], ERC_tot = emotion regulation checkList total scale, CPRS_DSM_tot = conners DSM-IV total scale) scores.

different recording sessions, supporting HMM inference as a robust methodology to investigate individual neural variability in the developing brain. This is particularly relevant considering the well-known difficulties in collecting good-quality neural data from young populations. Assessing the reliability of these neural indices is a fundamental step to study how they relate to individual differences in cognitive functioning. Our analyses served as an attempt to describe how different neural indices of brain dynamics are intrinsically related to broader measures of behavior and cognition in preschoolers. Overall, our results indicate that HMM-derived metrics show sex-related differences and predict CC measures. We discuss these results further in the following sections.

6 | SEX, BUT NOT AGE, EXPLAINS DIFFERENCES IN INDIVIDUAL NEURAL HALLMARKS

We observed sex-related differences in almost all the HMM-derived indices. This is in line with previous studies that found differences in static (Ritchie et al., 2018) and dynamic (Scofield et al., 2019) functional connectivity between girls and boys. For instance, Scofield et al. (2019) found that school-aged boys show greater dwell time in states related to the ventral attention network, DMN and somatomotor network, before switching to another state. In a similar vein, our analysis

revealed that, compared to girls, boys tend to switch more frequently between states, especially toward states that might be considered task-negative or default-mode like (state 2 involves activations over the precuneus, which is reminiscent of a posterior default-mode activation; Raichle, 2015) and spend on average more time in almost all the states including state 1 (anterior default-mode like). Conversely, girls switch less frequently between states but mostly toward CCN-like states, where they spend more time: state 5 (prefrontal) and state 4 (occipito-parietal, somatomotor). Interestingly, both prefrontal and parietal areas have been proposed as two core hubs underlying high-order cognitive functioning. For instance, individual differences in reasoning and working memory abilities might rely on the interplay between parietal and frontal association cortices, as well as other structural and functional parameters like their volume, gray matter density and mean diffusivity (Gur et al., 2021; Jung & Haier, 2007; Li & Tian, 2014). Additionally, the fronto-parietal network is considered a modal controllability hub, which is the ability of a given network to drive the whole brain into states that are difficult to reach, such as those entered under high cognitive demand (Gu et al., 2015). Greater engagement (fractional occupancy) of these states in girls might explain their reduced SR and entropy rates compared to boys. Therefore, we speculate that these sex-related differences in brain dynamics may heighten boys' neurobiological risk of atypical developmental trajectories associated with compromised CC (Bölte et al., 2023). Contrary to our expectations (Kupis et al., 2021) we did

not find age-related differences in the HMM-derived indices. This could be due to the restricted age-range considered in the present study (i.e., 4–6 years).

6.1 | Brain state transitions are associated with CC

The preschool period is a sensitive window for the development of CC, particularly due to increasing patterns of connectivity between the prefrontal cortex, the anterior cingulate cortex, and the parietal cortex (Fiske & Holmboe, 2019). In the present study, we found that specific resting-state patterns of brain state transitions are associated with CC, as assessed using parental questionnaires. More specifically, we found that a higher probability of transitioning into state 6 (fronto-temporal) was associated with better scores in questionnaires assessing executive functioning in everyday life (BRIEF-P; Gioia et al., 1996), behavioral difficulties (CPRS; Conners et al., 1998) and emotion regulation abilities (ERC; Molina et al., 2014). On the contrary, we found that a higher probability of transitioning into state 2 (posterior default-mode like) was associated with worse scores in the same measures. Overall, these findings build on previous studies supporting the important role of the prefrontal cortex for CC development (Friedman & Robbins, 2022). Moreover, it confirms and extends previous findings suggesting the relevance of brain dynamics for CC within the preschooler period (Cabral et al., 2017; Kupis et al., 2021). Specifically, previous evidence showed that adults performing differently in CC tasks displayed different brain state transitions (Cabral et al., 2017) and that, generally, brain state transitions relate to subject-specific cognitive traits (Vidaurre et al., 2017). Within this framework, our findings suggest that a higher tendency to enter prefrontal states might favor the engagement of CC abilities in response to external demands (Emili Balaguer-Ballester et al., 2011).

Interestingly, we also found that a higher probability of transitioning into state 3 (occipito-temporal, somatomotor), was associated with better emotional regulation (ERC; Molina et al., 2014). State 3 activation involves areas associated with the ventral circuit (fusiform area, occipital extrastriate and superior temporal sulcus) along with right frontal areas and might overlap with the social pathway recently proposed by Pitcher and Ungerleider (2021). This latter network is specialized for processing dynamic aspects of social perception. Therefore, we can hypothesize a relationship between the at-rest functional activation of this network and the way young children manage their emotion regulation in social contexts. Nevertheless, this hypothesis is speculative and would require further investigation.

As a general note, the transition probabilities between brain states offer valuable insights into the behavior of cognitive networks, reflecting in turn the fluidity and adaptability of cognitive processes. Frequent and predictable transitions between specific states may suggest a flexible and adaptive cognitive system, indicative of efficient CC (e.g., Dosenbach et al., 2007). Conversely, lower transition probabilities might point to a more rigid or specialized network behavior, potentially reflecting difficulties in cognitive flexibility or control (Sporns, 2013). For typically developing preschoolers, our findings

indicate that higher transitions toward brain states involving fronto-parietal–temporal areas are associated with more efficient CC, with this effect being more pronounced in girls than in boys. Importantly, deviations from typical state transitions could signal less efficient CC even in the absence of formal clinical diagnoses (Petersen & Posner, 2012). In this regard, we observed that higher transition probabilities toward a DMN-like state are more frequent in boys and associated with lower CC. In populations with CC difficulties, such as those with ADHD or schizophrenia, the states' temporal dynamics might exhibit prolonged dwell times in certain states or reduced flexibility in transitions. These patterns can manifest as difficulties in maintaining attention or switching tasks, which are central to altered CC (Anticevic et al., 2014; Fair et al., 2010).

Overall, it is interesting to note that we found relationships between state transition probabilities and parental questionnaires scores, but no relationship with direct cognitive measures. This might depend on the highly contextual-dependent performance of young children and, in turn, on the low test–retest reliability of such neuropsychological measures, which may not be sensitive enough to individual differences (Karalunas et al., 2020). Consequently, upcoming studies should aim to find more sensitive measures for assessing cognitive abilities in preschoolers.

Notably, in contrast to previous studies on adults (Nomi et al., 2017; Taghia et al., 2018; Vidaurre et al., 2017), and older school-aged children (Zdorovtsova et al., 2023), we only found state transition probabilities to be associated with CC, while we found no relationship with other HMM-derived neural indices (SR, entropy rates, and fractional occupancies). One potential explanation is that state transition patterns might represent a prominent and more sensitive feature of CC development during the preschool-age period compared to other neural indices. Indeed, during this time the brain undergoes substantial functional modifications, including changes in interregional activity (Brown & Jernigan, 2012), that may be better captured by state transitions rather than the other HMM indices. Future studies should address this point using different CC measures. Finally, task-evoked HMM-derived indices might provide a complementary view (Medaglia et al., 2018).

6.2 | Limitations and future directions

The present study has some potential limitations. First, the first-order Markovian assumption of our HMM estimation implies that the future state depends on the current state. However, this assumption is potentially restricting. For instance, it ignores the potential influence of past states on future behavior and fails to capture non-Markovian dynamics (Trujillo-Barreto et al., 2024). This can lead to inaccurate predictions in systems where past interactions impact future outcomes. To circumvent these issues, future studies could adopt more flexible approaches such as higher-order HMM to incorporate more complex temporal dependencies. In this vein, a prominent solution is generalized hidden semi-Markov models that allow explicit specification of the duration model (Trujillo-Barreto et al., 2024).

Second, reliability of the HMM-derived metrics was tested using two resting-state sessions recorded on the same day. This is justified since the measures we focus on are dynamic and fluctuate in the range of milliseconds, but future studies should confirm our results by recording the resting-state sessions on different days.

Finally, future studies should include children at-risk for neurodevelopmental conditions such as ADHD, in order to better understand if and how deviations from typical state transitions could represent a potential marker of poor CC.

7 | CONCLUSIONS

We inferred a six-state Multivariate Gaussian HMM using resting-state hdEEG brain activity in a developmental, preschool-aged sample (4–6 years). These brain state characteristics derived from the HMM were reliable across different recording sessions, allowing their use as individual neural hallmarks, and differed between boys and girls. Moreover, transition patterns between states were predictive of individual differences on CC measures (parental questionnaires scores). In line with previous evidence, the current study supports the importance of resting-state brain dynamics as an important scaffold for behavior and cognition. Moreover, for the first time, we extend these findings to the preschool period and suggest that brain state transitions might be particularly salient during this developmental window. Therefore, brain state transitions should be targeted by future studies investigating neurodevelopmental trajectories and early markers of neurodivergent development.

CONFLICT OF INTEREST STATEMENT

The authors declare no competing interests.

ORCID

Lisa Toffoli [iD] https://orcid.org/0000-0002-1664-7744
Gian Marco Duma [iD] https://orcid.org/0000-0002-0778-3920

REFERENCES

Allen, E. A., Damaraju, E., Plis, S. M., Erhardt, E. B., Eichele, T., & Calhoun, V. D. (2014). Tracking whole-brain connectivity dynamics in the resting state. *Cerebral Cortex*, 24(3), 663–676.

Alvarez, J. A., & Emory, E. (2006). Executive function and the frontal lobes: A meta-analytic review. *Neuropsychology Review*, 16, 17–42. https://doi.org/10.1007/s11065-006-9002-x

Anticevic, A., Yang, G., Savic, A., Murray, J. D., Cole, M. W., Repovs, G., Pearlson, G. D., & Glahn, D. C. (2014). Mediodorsal and visual thalamic connectivity differ in schizophrenia and bipolar disorder with and without psychosis history. *Schizophrenia Bulletin*, 40(6), 1227–1243. https://doi.org/10.1093/schbul/sbu100

Ashburner, J., Barnes, G., Chen, C.-C., Daunizeau, J., Flandin, G., Friston, K., Kiebel, S., Kilner, J., Litvak, V., & Moran, R. (2014). SPM12 manual. *Wellcome Trust Centre for Neuroimaging*. London, UK. 2464(4). https://www.researchgate.net/profile/Amirhossein_Jafarian/publication/355544981_SPM12_Manual/links/6176b29c3c987366c3e371fa/SPM12-Manual.pdf

Avery, E. W., Yoo, K., Rosenberg, M. D., Greene, A. S., Gao, S., Na, D. L., Scheinost, D., Constable, T. R., & Chun, M. M. (2020). Distributed patterns of functional connectivity predict working memory performance in novel healthy and memory-impaired individuals. *Journal of Cognitive Neuroscience*, 32(2), 241–255. https://doi.org/10.1162/jocn_a_01487

Baker, A. P., Brookes, M. J., Rezek, I. A., Smith, S. M., Behrens, T., Probert Smith, P. J., & Woolrich, M. (2014). Fast transient networks in spontaneous human brain activity. *eLife*, 3, e01867. https://doi.org/10.7554/eLife.01867

Balaguer-Ballester, E., Lapish, C. C., Seamans, J. K., & Durstewitz, D. (2011). Attracting dynamics of frontal cortex ensembles during memory-guided decision-making. *PLoS Computational Biology*, 7(5), e1002057. https://doi.org/10.1371/journal.pcbi.1002057

Barnes, J. J., Woolrich, M. W., Baker, K., Colclough, G. L., & Astle, D. E. (2016). Electrophysiological measures of resting state functional connectivity and their relationship with working memory capacity in childhood. *Developmental Science*, 19(1), 19–31. https://doi.org/10.1111/desc.12297

Bassett, D. S., Meyer-Lindenberg, A., Achard, S., Duke, T., & Bullmore, E. (2006). Adaptive reconfiguration of fractal small-world human brain functional networks. *Proceedings of the National Academy of Sciences*, 103(51), 19518–19523. https://doi.org/10.1073/pnas.0606005103

Bell, A. J., & Sejnowski, T. J. (1995). An information-maximization approach to blind separation and blind deconvolution. *Neural Computation*, 7(6), 1129–1159. https://doi.org/10.1162/neco.1995.7.6.1129

Bisiacchi, P. S., Cendron, M., Gugliotta, M., Tressoldi, P. E., & Vio, C. B. V. N. (2005). *BVN 5-11 Batteria di Valutazione Neuropsicologica per l'età Evolutiva* (Vol. 1, pp. 1–324). Erickson. Retrieved from https://hdl.handle.net/11381/1445131

Bölte, S., Neufeld, J., Marschik, P. B., Williams, Z. J., Gallagher, L., & Lai, M. C. (2023). Sex and gender in neurodevelopmental conditions. *Nature Reviews Neurology*, 19(3), 136–159. https://doi.org/10.1038/s41582-023-00774-6

Braem, S., & Egner, T. (2018). Getting a grip on cognitive flexibility. *Current Directions in Psychological Science*, 27(6), 470–476. https://doi.org/10.1177/0963721418787475

Braun, U., Schäfer, A., Walter, H., Erk, S., Romanczuk-Seiferth, N., Haddad, L., Schweiger, J. I., Grimm, O., Heinz, A., Tost, H., Meyer-Lindenberg, A., & Bassett, D. S. (2015). Dynamic reconfiguration of frontal brain networks during executive cognition in humans. *Proceedings of the National Academy of Sciences of the United States of America*, 112(37), 11678–11683. https://doi.org/10.1073/pnas.1422487112

Bressler, S. L., & Tognoli, E. (2006). Operational principles of neurocognitive networks. *International Journal of Psychophysiology*, 60(2), 139–148. https://doi.org/10.1016/j.ijpsycho.2005.12.008

Breukelaar, I. A., Griffiths, K. R., Harris, A., Foster, S. L., Williams, L. M., & Korgaonkar, M. S. (2020). Intrinsic functional connectivity of the default mode and cognitive control networks relate to change in behavioral performance over two years. *Cortex*, 132, 180–190. https://doi.org/10.1016/j.cortex.2020.08.014

Brookes, M. J., O'Neill, G. C., Hall, E. L., Woolrich, M. W., Baker, A., Corner, S. P., Robson, S. E., Morris, P. G., & Barnes, G. R. (2014). Measuring temporal, spectral and spatial changes in electrophysiological brain network connectivity. *NeuroImage*, 91, 282–299. https://doi.org/10.1016/j.neuroimage.2013.12.066

Brookes, M. J., Woolrich, M., Luckhoo, H., Price, D., Hale, J. R., Stephenson, M. C., Barnes, G. R., Smith, S. M., & Morris, P. G. (2011). Investigating the electrophysiological basis of resting state networks using magnetoencephalography. *Proceedings of the National Academy of Sciences of the United States of America*, 108(40), 16783–16788. https://doi.org/10.1073/pnas.1112685108

Brown, T. T., & Jernigan, T. L. (2012). Brain development during the preschool years. *Neuropsychology Review*, 22, 313–333. https://doi.org/10.1007/s11065-012-9214-1

Bürkner, P. C. (2017). brms: An R package for Bayesian multilevel models using Stan. *Journal of Statistical Software*, 80, 1–28. https://doi.org/10.18637/jss.v080.i01

Cabral, J., Vidaurre, D., Marques, P., Magalhães, R., Silva Moreira, P., Miguel Soares, J., Deco, G., Sousa, N., & Kringelbach, M. L. (2017). Cognitive performance in healthy older adults relates to spontaneous switching between states of functional connectivity during rest. *Scientific Reports*, 7(1), 5135. https://doi.org/10.1038/s41598-017-05425-7

Cai, W., Chen, T., Szegletes, L., Supekar, K., & Menon, V. (2018). Aberrant time-varying cross-network interactions in children with attention-deficit/hyperactivity disorder and the relation to attention deficits. *Biological Psychiatry: Cognitive Neuroscience and Neuroimaging*, 3(3), 263–273. https://doi.org/10.1016/j.bpsc.2017.10.005

Colclough, G. L., Brookes, M. J., Smith, S. M., & Woolrich, M. W. (2015). A symmetric multivariate leakage correction for MEG connectomes. *NeuroImage*, 117, 439–448. https://doi.org/10.1016/j.neuroimage.2015.03.071

Comer, J. S., Roy, A. K., Furr, J. M., Gotimer, K., Beidas, R. S., Dugas, M. J., & Kendall, P. C. (2009). The intolerance of uncertainty scale for children: A psychometric evaluation. *Psychological Assessment*, 21(3), 402–411. https://doi.org/10.1037/a0016719

Conners, C. K., Sitarenios, G., Parker, J. D., & Epstein, J. N. (1998). The revised Conners' Parent Rating Scale (CPRS-R): Factor structure, reliability, and criterion validity. *Journal of Abnormal Child Psychology*, 26, 257–268. https://doi.org/10.1023/A:1022602400621

Cui, Z., Stiso, J., Baum, G. L., Kim, J. Z., Roalf, D. R., Betzel, R. F., Gu, S., Lu, Z., Xia, C. H., & He, X. (2020). Optimization of energy state transition trajectory supports the development of executive function during youth. *Elife*, 9, e53060. https://doi.org/10.7554/eLife.53060

Dammu, P. S., & Bapi, R. S. (2019). Temporal dynamics of the brain using variational bayes hidden Markov models: Application in autism. In *Pattern Recognition and Machine Intelligence: 8th International Conference, PReMI 2019, Tezpur, India, December 17-20, 2019, Proceedings, Part I* (pp. 121-130). Springer International Publishing. https://doi.org/10.1007/978-3-030-34869-4_14

Dang, S., Chaudhury, S., Lall, B., & Roy, P. K. (2017). Learning effective connectivity from fMRI using autoregressive hidden Markov model with missing data. *Journal of Neuroscience Methods*, 278, 87–100. https://doi.org/10.1016/j.jneumeth.2016.12.019

Dash, D. P., Kolekar, M. H., & Jha, K. (2020). Multi-channel EEG based automatic epileptic seizure detection using iterative filtering decomposition and hidden Markov model. *Computers in Biology and Medicine*, 116, 103571. https://doi.org/10.1016/j.compbiomed.2019.103571

Delorme, A., & Makeig, S. (2004). EEGLAB: An open source toolbox for analysis of single-trial EEG dynamics including independent component analysis. *Journal of Neuroscience Methods*, 134(1), 9–21. https://doi.org/10.1016/j.jneumeth.2003.10.009

Diamond, A. (2013). Executive functions. *Annual Review of Psychology*, 64, 135–168. https://doi.org/10.1146/annurev-psych-113011-143750

Ding, L., Shou, G., Cha, Y. H., Sweeney, J. A., & Yuan, H. (2022). Brain-wide neural co-activations in resting human. *NeuroImage*, 260, 119461. https://doi.org/10.1016/j.neuroimage.2022.119461

Dosenbach, N. U. F., Fair, D. A., Miezin, F. M., Cohen, A. L., Wenger, K. K., Dosenbach, R. A. T., Fox, M. D., Snyder, A. Z., Vincent, J. L., Raichle, M. E., Schlaggar, B. L., & Petersen, S. E. (2007). Distinct brain networks for adaptive and stable task control in humans. *Proceedings of the National Academy of Sciences of the United States of America*, 104(26), 11073–11078. https://doi.org/10.1073/pnas.0704320104

Duma, G. M., Danieli, A., Mattar, M. G., Baggio, M., Vettorel, A., Bonanni, P., & Mento, G. (2022). Resting state network dynamic reconfiguration and neuropsychological functioning in temporal lobe epilepsy: An HD-EEG investigation. *Cortex*, 157, 1–13. https://doi.org/10.1016/j.cortex.2022.08.010

Duma, G. M., Di Bono, M. G., & Mento, G. (2021). Grounding adaptive cognitive control in the intrinsic, functional brain organization: An HD-EEG resting state investigation. *Brain Sciences*, 11(11), 1513. https://doi.org/10.3390/brainsci11111513

Dwyer, D. B., Harrison, B. J., Yücel, M., Whittle, S., Zalesky, A., Pantelis, C., Allen, N. B., & Fornito, A. (2014). Large-scale brain network dynamics supporting adolescent cognitive control. *Journal of Neuroscience*, 34(42), 14096–14107. https://doi.org/10.1523/JNEUROSCI.1634-14.2014

Eickhoff, S. B., Bzdok, D., Laird, A. R., Roski, C., Caspers, S., Zilles, K., & Fox, P. T. (2011). Co-activation patterns distinguish cortical modules, their connectivity and functional differentiation. *NeuroImage*, 57(3), 938–949. https://doi.org/10.1016/j.neuroimage.2011.05.021

Fair, D. A., Dosenbach, N. U., Church, J. A., Cohen, A. L., Brahmbhatt, S., Miezin, F. M., Barch, D. M., Raichle, M. E., Petersen, S. E., & Schlaggar, B. L. (2007). Development of distinct control networks through segregation and integration. *Proceedings of the National Academy of Sciences of the United States of America*, 104(33), 13507–13512. https://doi.org/10.1073/pnas.0705843104

Fair, D. A., Posner, J., Nagel, B. J., Bathula, D., Dias, T. G. C., Mills, K. L., Blythe, M. S., Giwa, A., Schmitt, C. F., & Nigg, J. T. (2010). Atypical default network connectivity in youth with attention-deficit/hyperactivity disorder. *Biological Psychiatry*, 68(12), 1084–1091. https://doi.org/10.1016/j.biopsych.2010.07.003

Fiske, A., & Holmboe, K. (2019). Neural substrates of early executive function development. *Developmental Review*, 52, 42–62. https://doi.org/10.1016/j.dr.2019.100866

Fonov, V., Evans, A. C., Botteron, K., Almli, C. R., McKinstry, R. C., Collins, D. L., & Brain Development Cooperative Group. (2011). Unbiased average age-appropriate atlases for pediatric studies. *NeuroImage*, 54(1), 313–327. https://doi.org/10.1016/j.neuroimage.2010.07.033

Friedman, N. P., & Robbins, T. W. (2022). The role of prefrontal cortex in cognitive control and executive function. *Neuropsychopharmacology*, 47(1), 72–89. https://doi.org/10.1038/s41386-021-01132-0

Gioia, G. A., Andrwes, K., & Isquith, P. K. (1996). *Behavior rating inventory of executive function-preschool version (BRIEF-P)*. Psychological Assessment Resources.

Goucher-Lambert, K., & McComb, C. (2019). Using hidden Markov models to uncover underlying states in neuroimaging data for a design ideation task. In *Proceedings of the Design Society: International Conference on Engineering Design* (Vol. 1, No. 1, pp. 1873-1882). Cambridge University Press. https://doi.org/10.1017/dsi.2019.193

Gu, S., Pasqualetti, F., Cieslak, M., Telesford, Q. K., Yu, A. B., Kahn, A. E., Medaglia, J. D., Vettel, J. M., Miller, M. B., & Grafton, S. T. (2015). Controllability of structural brain networks. *Nature Communications*, *6*(1), 8414. https://doi.org/10.1038/ncomms9414

Gur, R. C., Butler, E. R., Moore, T. M., Rosen, A. F., Ruparel, K., Satterthwaite, T. D., Roalf, D. R., Gennatas, E. D., Bilker, W. B., & Shinohara, R. T. (2021). Structural and functional brain parameters related to cognitive performance across development: Replication and extension of the parieto-frontal integration theory in a single sample. *Cerebral Cortex*, *31*(3), 1444–1463. https://doi.org/10.1093/cercor/bhaa282

Hall, W. S., & Hall, W. S. (1994). *Boundary element method* (pp. 61–83). Springer. https://doi.org/10.1007/978-94-011-0784-6_3

Hauk, O. (2004). Keep it simple: A case for using classical minimum norm estimation in the analysis of EEG and MEG data. *NeuroImage*, *21*(4), 1612–1621. https://doi.org/10.1016/j.neuroimage.2003.12.018

Hawkins, E., Akarca, D., Zhang, M., Brkić, D., Woolrich, M., Baker, K., & Astle, D. (2020). Functional network dynamics in a neurodevelopmental disorder of known genetic origin. *Human Brain Mapping*, *41*(2), 530–544. https://doi.org/10.1002/hbm.24820

Hussain, S., Langley, J., Seitz, A. R., Hu, X. P., & Peters, M. A. (2023). A novel hidden Markov approach to studying dynamic functional connectivity states in human neuroimaging. *Brain Connectivity*, *13*(3), 154–163. https://doi.org/10.1089/brain.2022.0031

Hutchison, R. M., & Morton, J. B. (2016). It's a matter of time: Reframing the development of cognitive control as a modification of the brain's temporal dynamics. *Developmental Cognitive Neuroscience*, *18*, 70–77. https://doi.org/10.1016/j.dcn.2015.08.006

Hutchison, R. M., Womelsdorf, T., Allen, E. A., Bandettini, P. A., Calhoun, V. D., Corbetta, M., Della Penna, S., Duyn, J. H., Glover, G. H., & Gonzalez-Castillo, J. (2013). Dynamic functionalconnectivity: Promise, issues, and interpretations. *NeuroImage*, *80*, 360–378. https://doi.org/10.1016/j.neuroimage.2013.05.079

Ingram, B. T., Mayhew, S. D., & Bagshaw, A. P. (2024). Brain state dynamics differ between eyes open and eyes closed rest. *Human Brain Mapping*, *45*(10), e26746. https://doi.org/10.1002/hbm.26746

Jones, J. S., CALM Team, & Astle, D. E. (2022). Segregation and integration of the functional connectome in neurodevelopmentally 'at risk' children. *Developmental Science*, *25*(3), e13209. https://doi.org/10.1111/desc.13209

Jung, R. E., & Haier, R. J. (2007). The parieto-frontal integration theory (P-FIT) of intelligence: Converging neuroimaging evidence. *Behavioral and Brain Sciences*, *30*(2), 135–154. https://doi.org/10.1017/S0140525X07001185

Karalunas, S. L., Bierman, K. L., & Huang-Pollock, C. L. (2020). Test–retest reliability and measurement invariance of executive function tasks in young children with and without ADHD. *Journal of Attention Disorders*, *24*(13), 1891–1904. https://doi.org/10.1177/1087054715627488

Kruschke, J. K. (2018). Rejecting or accepting parameter values in Bayesian estimation. *Advances in Methods and Practices in Psychological Science*, *1*(2), 270–280. https://doi.org/10.1177/2515245918771304

Kupis, L., Goodman, Z. T., Kornfeld, S., Hoang, S., Romero, C., Dirks, B., Dehoney, J., Chang, C., Spreng, R. N., & Nomi, J. S. (2021). Brain dynamics underlying cognitiveflexibility across the lifespan. *Cerebral Cortex*, *31*(11), 5263–5274. https://doi.org/10.1093/cercor/bhab156

Li, C., & Tian, L. (2014). Association between resting-state coactivation in the parieto-frontal network and intelligence during late childhood and adolescence. *American Journal of Neuroradiology*, *35*(6), 1150–1156. https://doi.org/10.3174/ajnr.A3850

Liu, X., & Duyn, J. H. (2013). Time-varying functional network information extracted from brief instances of spontaneous brain activity. *Proceedings of the National Academy of Sciences*, *110*(11), 4392–4397. https://doi.org/10.1073/pnas.1216856110

Makowski, D., Ben-Shachar, M. S., & Lüdecke, D. (2019). bayestestR: Describing effects and their uncertainty, existence and significance within the Bayesian framework. *Journal of Open Source Software*, *4*(40), 1541. https://doi.org/10.21105/joss.01541

Mansouri, F. A., Koechlin, E., Rosa, M. G., & Buckley, M. J. (2017). Managing competing goals—A key role for the frontopolar cortex. *Nature Reviews Neuroscience*, *18*(11), 645–657.

Marano, A., Innocenzi, M., & Devescovi, A. (2014). BRIEF-P behavior rating inventory of executive function–preschool version G. A. Gioia, K. A. Espy, P. K. Isquith. In *BRIEF-P Behavior Rating Inventory of Executie Function*. *Peschool Version*. *Adattamento italianodi Assunta Marano*, *Margherita Innocenzi e Antonella Devescovi* (pp. 9-74). Hogrefe Italia. Retrieved from https://hdl.handle.net/11573/567929

Marzetti, L. (2023). EEG brain networks identified by hidden Markov model and their relation to TMS-evoked MEP amplitudes. *Brain Stimulation: Basic, Translational, and Clinical Research in Neuromodulation*, *16*(1), 119–120. https://doi.org/10.1016/j.brs.2023.01.023

Maya Piedrahita, M. C. (2021). Supported diagnosis of ADHD from EEG signals based on hidden Markov models and probability product kernels. Retrieved from https://hdl.handle.net/11059/13162

Medaglia, J. D., Satterthwaite, T. D., Kelkar, A., Ciric, R., Moore, T. M., Ruparel, K., Gur, R. C., Gur, R. E., & Bassett, D. S. (2018). Brain state expression and transitions are related to complex executive cognition in normative neuro development. *NeuroImage*, *166*, 293–306. https://doi.org/10.1016/j.neuroimage.2017.10.048

Michel, C. M., & Murray, M. M. (2012). Towards the utilization of EEG as a brain imaging tool. *NeuroImage*, *61*(2), 371–385. https://doi.org/10.1016/j.neuroimage.2011.12.039

Miyake, A., & Friedman, N. P. (2012). The nature and organization of individual differences in executive functions: Four general conclusions. *Current Directions in Psychological Science*, *21*(1), 8–14. https://doi.org/10.1177/0963721411429458

Molina, P., Sala, M. N., Zappulla, C., Bonfigliuoli, C., Cavioni, V., Zanetti, M. A., Baiocco, R., Laghi, F., Pallini, S., De Stasio, S., Raccanello, D., & Cicchetti, D. (2014). The emotion regulation checklist—Italian translation. Validation of parent and teacher versions. *European Journal of Developmental Psychology*, *11*(5), 624–634. https://doi.org/10.1080/17405629.2014.898581

Niendam, T. A., Laird, A. R., Ray, K. L., Dean, Y. M., Glahn, D. C., & Carter, C. S. (2012). Meta-analytic evidence for a superordinate cognitive control network subserving diverse executive functions. *Cognitive, Affective, & Behavioral Neuroscience*, *12*, 241–268. https://doi.org/10.3758/s13415-011-0083-5

Nobile, M., Alberti, B., & Zuddas, A. (Eds.). (2007). *Conners' rating scales-revise. Manuale [Conners' rating scales-revised, manual]*. Giunti O.S.

Nomi, J. S., Vij, S. G., Dajani, D. R., Steimke, R., Damaraju, E., Rachakonda, S., Calhoun, V. D., & Uddin, L. Q. (2017). Chronnectomic patterns and neural flexibility underlie executive function. *NeuroImage*, *147*, 861–871. https://doi.org/10.1016/j.neuroimage.2016.10.026

Obermaier, B., Guger, C., Neuper, C., & Pfurtscheller, G. (2001). Hidden Markov models for online classification of single trial EEG data. *Pattern Recognition Letters*, *22*(12), 1299–1309. https://doi.org/10.1016/S0167-8655(01)00075-7

Perrin, F., Pernier, J., Bertrand, O., & Echallier, J. F. (1989). Spherical splines for scalp potential and current density mapping. *Electroencephalography and Clinical Neurophysiology*, *72*(2), 184–187. https://doi.org/10.1016/0013-4694(89)90180-6

Petersen, S. E., & Posner, M. I. (2012). The attention system of the human brain: 20 years after. *Annual Review of Neuroscience*, *35*(1), 73–89. https://doi.org/10.1146/annurev-neuro-062111-150525

Pitcher, D., & Ungerleider, L. G. (2021). Evidence for a third visual pathway specialized for social perception. *Trends in Cognitive Sciences*, *25*(2), 100–110. https://doi.org/10.1016/j.tics.2020.11.006

Poole, V. N., Robinson, M. E., Singleton, O., DeGutis, J., Milberg, W. P., McGlinchey, R. E., Salat, D. H., & Esterman, M. (2016). Intrinsic functional connectivity predicts individual differences in distractibility. *Neuropsychologia*, *86*, 176–182. https://doi.org/10.1016/j.neuropsychologia.2016.04.023

Qualtrics Provo, UT, USA. Retrieved from https://www.qualtrics.com

Quinn, A. J., Vidaurre, D., Abeysuriya, R., Becker, R., Nobre, A. C., & Woolrich, M. W. (2018). Task-evoked dynamic network analysis through hidden markov modeling. *Frontiers in Neuroscience*, *12*, 603. https://doi.org/10.3389/fnins.2018.00603

R Core Team. (2021). R: A language and environment for statistical computing. Supplemental Information References S, 1, 371–378. Retrieved from https://www.R-project.org/

Raichle, M. E. (2015). The brain's default mode network. *Annual Review of Neuroscience*, *38*, 433–447. https://doi.org/10.1146/annurev-neuro-071013-014030

Raven, J. C., & Court, J. H. (1938). *Raven's progressive matrices*. Western Psychological Services.

Ritchie, S. J., Cox, S. R., Shen, X., Lombardo, M. V., Reus, L. M., Alloza, C., Harris, M. A., Alderson, H. L., Hunter, S., & Neilson, E. (2018). Sex differences in theadult human brain: Evidence from 5216 UK biobank participants. *Cerebral Cortex*, *28*(8), 2959–2975. https://doi.org/10.1093/cercor/bhy109

Rottschy, C., Langner, R., Dogan, I., Reetz, K., Laird, A. R., Schulz, J. B., Fox, P. T., & Eickhoff, S. B. (2012). Modelling neural correlates of working memory: A coordinate-based meta-analysis. *NeuroImage*, *60*(1), 830–846. https://doi.org/10.1016/j.neuroimage.2011.11.050

Satterthwaite, T. D., Wolf, D. H., Erus, G., Ruparel, K., Elliott, M. A., Gennatas, E. D., Hopson, R., Jackson, C., Prabhakaran, K., & Bilker, W. B. (2013). Functional maturation of the executive system during adolescence. *Journal of Neuroscience*, *33*(41), 16249–16261. https://doi.org/10.1523/JNEUROSCI.2345-13.2013

Scofield, J. E., Johnson, J. D., Wood, P. K., & Geary, D. C. (2019). Latent resting-state network dynamics in boys and girls with attention-deficit/hyperactivity disorder. *PLoS One*, *14*(6), e0218891. https://doi.org/10.1371/journal.pone.0218891

Smith, S. M., Miller, K. L., Salimi-Khorshidi, G., Webster, M., Beckmann, C. F., Nichols, T. E., Ramsey, J. D., & Woolrich, M. W. (2011). Network modelling methods for FMRI. *NeuroImage*, *54*(2), 875–891. https://doi.org/10.1016/J.NEUROIMAGE.2010.08.063

Smith, S. M., Vidaurre, D., Beckmann, C. F., Glasser, M. F., Jenkinson, M., Miller, K. L., Nichols, T. E., Robinson, E. C., Salimi-Khorshidi, G., & Woolrich, M. W. (2013). Functional connectomics from resting-state fMRI. *Trends in Cognitive Sciences*, *17*(12), 666–682. https://doi.org/10.1016/j.tics.2013.09.016

Smitha, K. A., Akhil Raja, K., Arun, K. M., Rajesh, P. G., Thomas, B., Kapilamoorthy, T. R., & Kesavadas, C. (2017). Resting state fMRI: A review on methods in resting state connectivity analysis and resting state networks. *The Neuroradiology Journal*, *30*(4), 305–317. https://doi.org/10.1177/1971400917697342

Sporns, O. (2013). Structure and function of complex brain networks. *Dialogues in Clinical Neuroscience*, *15*(3), 247–262. https://doi.org/10.31887/DCNS.2013.15.3/osporns

Stone, J. V. (2002). Independent component analysis: An introduction. *Trends in Cognitive Sciences*, *6*(2), 59–64. https://doi.org/10.1016/S1364-6613(00)01813-1

Taghia, J., Cai, W., Ryali, S., Kochalka, J., Nicholas, J., Chen, T., & Menon, V. (2018). Uncovering hidden brain state dynamics that regulate performance and decision-making during cognition. *Nature Communications*, *9*(1), 2505. https://doi.org/10.1038/s41467-018-04723-6

Tang, E., Giusti, C., Baum, G. L., Gu, S., Pollock, E., Kahn, A. E., Roalf, D. R., Moore, T. M., Ruparel, K., & Gur, R. C. (2017). Developmental increases in white matter network controllability support a growing diversity of brain dynamics. *Nature Communications*, *8*(1), 1252. https://doi.org/10.1038/s41467-017-01254-4

Trujillo-Barreto, N. J., Araya, D., Astudillo, A., & El-Deredy, W. (2024). Explicit modeling of brain state duration using hidden semi Markov models in EEG data. *IEEE Access*. https://doi.org/10.1109/ACCESS.2024.3354711

Uddin, L. Q., Supekar, K., & Menon, V. (2010). Typical and atypical development of functional human brain networks: Insights from resting-state FMRI. *Frontiers in Systems Neuroscience*, *4*, 1447. https://doi.org/10.3389/fnsys.2010.00021

Usai, M. C., Viterbori, P., Gandolfi, E., & Traverso, L. (2017). *FE-PS 2-6: Batteria per la valutazione delle funzioni esecutive in età prescolare*. Edizioni Centro Studi Erickson.

Van Veen, B. D., Van Drongelen, W., Yuchtman, M., & Suzuki, A. (1997). Localization of brain electrical activity via linearly constrained minimum variance spatial filtering. *IEEE Transactions on Biomedical Engineering*, *44*(9), 867–880.

Vanderwal, T., Kelly, C., Eilbott, J., Mayes, L. C., & Castellanos, F. X. (2015). Inscapes: A movie paradigm to improve compliance in functional magnetic resonance imaging. *NeuroImage*, *122*, 222–232. https://doi.org/10.1016/j.neuroimage.2015.07.069

Vehtari, A., Gelman, A., Gabry, J., & Yao, Y. (2021). Package 'loo'. Efficient leave-one-out cross-validation and WAIC for Bayesian models.

Vehtari, A., Gelman, A., Simpson, D., Carpenter, B., & Bürkner, P. C. (2021). Rank-normalization, folding, and localization: An improved $\hat{R}$ for assessing convergence of MCMC (with discussion). *Bayesian Analysis*, *16*(2), 667–718. https://doi.org/10.1214/20-BA1221

Vidaurre, D., Abeysuriya, R., Becker, R., Quinn, A. J., Alfaro-Almagro, F., Smith, S. M., & Woolrich, M. W. (2018). Discovering dynamic brain networks from big data in rest and task. *NeuroImage*, *180*, 646–656. https://doi.org/10.1016/j.neuroimage.2017.06.077

Vidaurre, D., Quinn, A. J., Baker, A. P., Dupret, D., Tejero-Cantero, A., & Woolrich, M. W. (2016). Spectrally resolved fast transient brain states in electrophysiological data. *NeuroImage*, *126*, 81–95. https://doi.org/10.1016/j.neuroimage.2015.11.047

Vidaurre, D., Smith, S. M., & Woolrich, M. W. (2017). Brain network dynamics are hierarchically organized in time. *Proceedings of the National Academy of Sciences*, *114*(48), 12827–12832. https://doi.org/10.1073/pnas.1705120114

Wens, V., Bourguignon, M., Goldman, S., Marty, B., Op de Beeck, M., Clumeck, C., Mary, A., Peigneux, P., Van Bogaert, P., & Brookes, M. J. (2014). Inter- and intra-subject variability of neuromagnetic resting state networks. *Brain Topography*, *27*, 620–634. https://doi.org/10.1007/s10548-014-0364-8

Williams, N. J., Daly, I., & Nasuto, S. J. (2018). Markov model-based method to analyse time-varying networks in EEG task-related data. *Frontiers in Computational Neuroscience*, *12*, 76. https://doi.org/10.3389/fncom.2018.00076

Woolrich, M., Hunt, L., Groves, A., & Barnes, G. (2011). MEG beamforming using Bayesian PCA for adaptive data covariance matrix regularization. *NeuroImage*, *57*(4), 1466–1479. https://doi.org/10.1016/j.neuroimage.2011.04.041

Yuan, H., Ding, L., Zhu, M., Zotev, V., Phillips, R., & Bodurka, J. (2016). Reconstructing large-scale brain resting-state networks from high-resolution EEG: Spatial and temporal comparisons with fMRI. *Brain Connectivity*, *6*(2), 122–135. https://doi.org/10.1089/brain.2014.0336

Zdorovtsova, N., Young, E. J., Akarca, D., Anwyl-Irvine, A., RED Team, CALM Team, & Astle, D. E. (2023). The entropy of resting-state neural dynamics is a marker of general cognitive ability in childhood. *bioRxiv*, 2023-08. https://doi.org/10.1101/2023.08.08.552448

SUPPORTING INFORMATION

Additional supporting information can be found online in the Supporting Information section at the end of this article.